Combining Total Variation and Nonlocal Variational Models for Low-Light Image Enhancement

Daniel Torres[a], Catalina Sbert[b] and Joan Duran[c]

Department of Mathematics and Computer Science & IAC3, University of the Balearic Islands,
Cra. de Valldemossa, km. 7.5, E-07122 Palma, Illes Balears, Spain

Keywords: Low-Light Image Enhancement, Illumination Estimation, Reflectance Estimation, Retinex, Variational Method, Total Variation, Nonlocal Regularization.

Abstract: Images captured under low-light conditions impose significant limitations on the performance of computer vision applications. Therefore, improving their quality by discounting the effects of the illumination is crucial. In this paper, we present a low-light image enhancement method based on the Retinex theory. Our approach estimates illumination and reflectance in two steps. First, the illumination is obtained as the minimizer of an energy functional involving total variation regularization, which favours piecewise smooth solutions. Next, the reflectance component is computed as the minimizer of an energy functional involving contrast-invariant nonlocal regularization and a fidelity term preserving the largest gradients of the input image.

1 INTRODUCTION

Enhancing images captured under low-light conditions is crucial for many applications in computer vision. Various strategies have been proposed to tackle this problem (Wang et al., 2020), broadly classified into histogram equalization (Thepade et al., 2021; Paul et al., 2022), Retinex-based methods, fusion approaches (Fu et al., 2016a; Buades et al., 2020), and deep-learning techniques.

The Retinex theory (Land and McCann, 1971), which aims to explain and simulate how the human visual system perceives color independently of global illumination changes, has been an important basis for addressing low-light image enhancement. One of the most used models assumes that the observed image L is the product of the illumination T, which depicts the light intensity on the objects, and the reflectance R, which represents their physical characteristics:

$$L = R \circ T, \qquad (1)$$

where $\circ$ denotes pixel-wise multiplication. The illumination map is assumed to be smooth, while the reflectance component contains fine details and texture (Ng and Wang, 2011; Li et al., 2018).

Decomposing an image into illumination and reflectance is mathematically ill-posed. To address this issue, patch-based (Land and McCann, 1971), partial differential equations (Morel et al., 2010), center/surround (Jobson et al., 1996) and variational (Kimmel et al., 2001; Ng and Wang, 2011; Ma and Osher, 2012; Fu et al., 2016b; Guo et al., 2017; Gu et al., 2019) methods have been proposed.

Recently, the growing popularity of deep learning has lead to an increase in enhancement methods (Wei et al., 2018; Lv et al., 2021). However, the structure of these architectures is often non-intuitive, and their training and testing require high computational costs.

In this paper, we present a low-light image enhancement method taking into account the decomposition model given in (1). We propose to estimate illumination and reflectance separately. In the first step, the illumination component is obtained as the minimizer of an energy functional involving total variation (TV) regularization (Rudin et al., 1992), which favours piecewise smooth solutions. We assume that the channels of color images share the same illumination map. In a second step, the reflectance component is computed as the minimizer of an energy involving nonlocal regularization, which exploits image self-similarities, and a fidelity term preserving the large gradients of the input low-light image. Importantly, the nonlocal regularization depends on a weight function that is contrast-invariant.

---

[a] https://orcid.org/0009-0000-5829-8557
[b] https://orcid.org/0000-0003-1219-4474
[c] https://orcid.org/0000-0003-0043-1663

2 RELATED WORK

In the variational framework, the enhanced image is computed as the minimizer of an energy functional that comprises data-fidelity and regularization terms. The latter quantifies the smoothness of the solution by usually prescribing priors on the gradient of the illumination or reflectance components.

Kimmel et al. (Kimmel et al., 2001) pioneered a variational model to estimate the illumination in a multiscale setting. The illumination is assumed to be spatially smooth, thus gradient oscillations are penalized through L^2 norm. Ma et al. (Ma and Osher, 2012) introduced TV to directly compute the reflectance. On the contrary, Ng et al. (Ng and Wang, 2011) estimate illumination and reflectance simultaneously.

One of the most celebrated works is LIME (Guo et al., 2017). The authors propose a simple TV variational model to estimate T. Then, the reflectance is computed as $R = \frac{L}{T^\gamma + \varepsilon}$, where $\varepsilon > 0$ is a small constant and T^γ is the γ-corrected illumination. However, this strategy tends to amplify the noise, especially in dark regions. To overcome this issue, the authors propose as enhanced image $R \circ T^\gamma + R_d \circ (1 - T^\gamma)$, with R_d being the denoised reflectance. Note that any discrepancy in the illumination will impact the result.

Several other variational methods use logarithms to linearize (1). However, this transformation amplifies errors in gradient terms. In (Fu et al., 2016b), weights are introduced to address issues arising from large gradients when either R or T is small.

3 PROPOSED MODELS

In this section, we introduce our low-light image enhancement method. We estimate R and T separately using two different variational models. Let Ω be an open and bounded domain in $\mathbb{R}^n$, with $n \geq 2$.

3.1 TV Model for Luminance

Based on the classical ROF denoising model (Rudin et al., 1992), T is obtained as the minimizer of

$$\int_\Omega |DT| + \lambda \int_\Omega |T(x) - \hat{T}(x)|^2 dx, \qquad (2)$$

where $\int_\Omega |DT|$ is the TV semi-norm,

$\lambda > 0$ is a trade-off parameter, and $\hat{T}$ is an initial illumination estimate computed as $\hat{T}(x) = \max_{c \in \{R,G,B\}} L^c(x)$. The assumption underlying TV is that images consist of connected smooth regions (objects) surrounded by sharp contours. Accordingly, TV is a good prior for the luminance since it is optimal

Bookcase *Clothes rack* *Plush toy*

Figure 1: Pairs of low-light and ground-truth images from the LOL dataset (Wei et al., 2018) used for the experiments.

to reduce noise and reconstruct the main geometrical shape.

The energy in (2) is derived from LIME (Guo et al., 2017). However, we calculate the minimizer for the exact functional instead of an approximation.

3.2 Nonlocal Model for Reflectance

To estimate the reflectance component, we use nonlocal regularization (Gilboa and Osher, 2009; Duran et al., 2014), which assumes that images are self-similar, thereby preserving fine details and texture.

3.2.1 Basic Definitions and Notations

Let $u = (u_1, \ldots, u_C) : \Omega \to \mathbb{R}^C$ be a color image, where C denotes the number of channels. We also consider *nonlocal functions* $p = (p_1, \ldots, p_C) : \Omega \times \Omega \to \mathbb{R}^C$. Let $\omega : \Omega \times \Omega \to \mathbb{R}_{\geq 0}$ be a weight function, commonly defined in terms of differences between patches in u.

Definition 3.1. Given $u : \Omega \to \mathbb{R}^C$, its *nonlocal gradient* $\nabla_\omega u : \Omega \times \Omega \to \mathbb{R}^C$ is, for each $k \in \{1, \ldots, C\}$,

$$(\nabla_\omega u_k)(x,y) = \sqrt{\omega(x,y)}(u_k(y) - u_k(x)).$$

Given $p : \Omega \times \Omega \to \mathbb{R}^C$, its *nonlocal divergence* $div_\omega p : \Omega \to \mathbb{R}^C$ is, for each $k \in \{1, \ldots, C\}$,

$$(div_\omega p_k)(x)$$
$$= \int_\Omega \left(p_k(x,y)\sqrt{\omega(x,y)} - p_k(y,x)\sqrt{\omega(y,x)} \right) dy.$$

Definition 3.2. The *nonlocal vectorial total variation* (NLVTV) of $u \in L^1(\Omega; \mathbb{R}^C)$ is defined as

$$\int_\Omega |D_\omega u| = \sup_{p \in Y} \left\{ -\int_\Omega \langle u(x), (div_\omega p)(x) \rangle \, dx \right\},$$

with $Y = \{p \in C_c^\infty(\Omega \times \Omega; \mathbb{R}^C) : |p|_{\text{NL}}(x) \leq 1, \forall x \in \Omega\}$ and $|p|_{\text{NL}}(x) = \sqrt{\sum_{k=1}^C \int_\Omega (p_k(x,y))^2 \, dy}$.

3.2.2 Nonlocal Energy Functional

We propose to estimate the reflectance $R : \Omega \to \mathbb{R}^C$, usually $C = 3$, as the minimizer of the functional
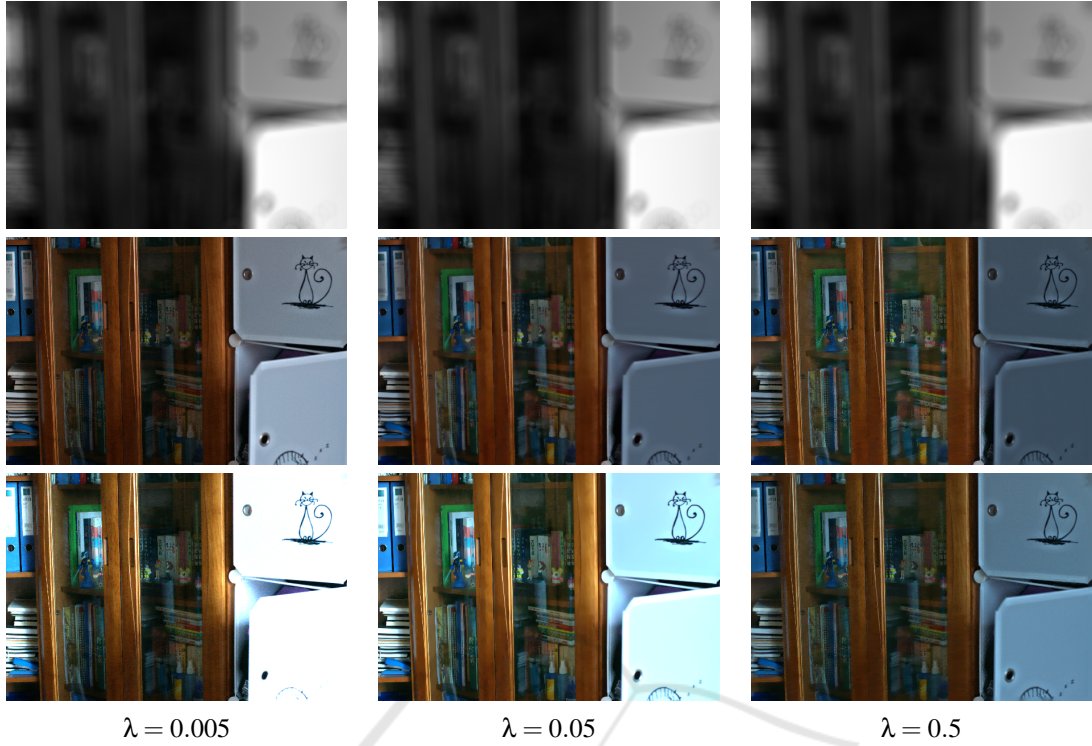
Figure 2: Visual impact of the trade-off parameter λ in (2). Each row contains the illumination, reflectance and enhanced image, respectively. We observe a piecewise smooth illumination in all cases. However, the differences are more noticeable in the reflectances and the enhanced images. Indeed, the smaller λ is, the brighter the result.

$$\beta \int_\Omega |D_\omega R| + \frac{\alpha}{2} \int_\Omega |\nabla R - G|^2 + \frac{1}{2} \int_\Omega |R - R_0|^2, \quad (3)$$

where $\alpha, \beta > 0$ are trade-off parameters, $\int_\Omega |D_\omega R|$ is the NLVTV, and R_0 is an initial estimate of the reflectance computed as $R_0(x) = \frac{L(x)}{T(x)+\varepsilon}$, with T being the minimizer of (2) and $\varepsilon > 0$ a small constant. The weight function ω will be defined in terms of differences between patches in L. Therefore, the underlying assumption behind NLVTV is that images are self-similar, making it a good prior for the reflectance.

The second term in (3) enforces closeness between the gradients of the reflectance and those of an adjusted version of the low-light image, strengthening the structural information. Following (Li et al., 2018), we define $G = \left(1 + \lambda_G e^{-|\nabla \hat{L}|/\sigma_G}\right) \circ \nabla \hat{L}$, with

$$\nabla \hat{L} = \begin{cases} 0 & \text{if } |\nabla L| < \varepsilon_G, \\ \nabla L & \text{otherwise,} \end{cases}$$

where σ_G controls the amplification rate of different gradients, λ_G controls the degree of the amplification, and ε_G is the threshold that filters small gradients.

3.2.3 Contrast-Invariant Weights

For the function $\omega : \Omega \times \Omega \to \mathbb{R}_{\geq 0}$ involved in NLVTV, we propose to use bilateral weights that con-

sider both the spatial closeness between points and the similarity in $L : \Omega \to \mathbb{R}^C$. This similarity is computed by considering a whole patch around each point and using the Euclidean distance across color channels:

$$d(L(x), L(y)) = \int_\Omega |(L(x+z) - \mu(x)) - (L(y+z) - \mu(y))|^2 dz, \quad (4)$$

where $\mu(x)$ denotes the mean value of the patch centered at x. This allows the distance (4) to be contrast invariant between the selected patches.

The weights are defined as

$$\omega(x,y) = \frac{1}{\Gamma(x)} \exp\left(-\frac{|x-y|^2}{h_{\text{spt}}^2} - \frac{d(L(x), L(y))}{h_{\text{sim}}^2}\right) \quad (5)$$

where $h_{\text{spt}}, h_{\text{sim}} > 0$ are filtering parameters that control how fast the weights decay with increasing spatial distance or dissimilarity between patches, respectively, and $\Gamma(x)$ is the normalization factor. Note that $0 < \omega(x,y) \leq 1$ and $\int_\Omega \omega(x,y)\,dy = 1$, but $\Gamma(x)$ breaks down the symmetry of ω. The average between very similar regions preserves the integrity of the image but reduces small oscillations, which contain noise.

For computational purposes, NLVTV is limited to interact only between points at a certain distance. Let
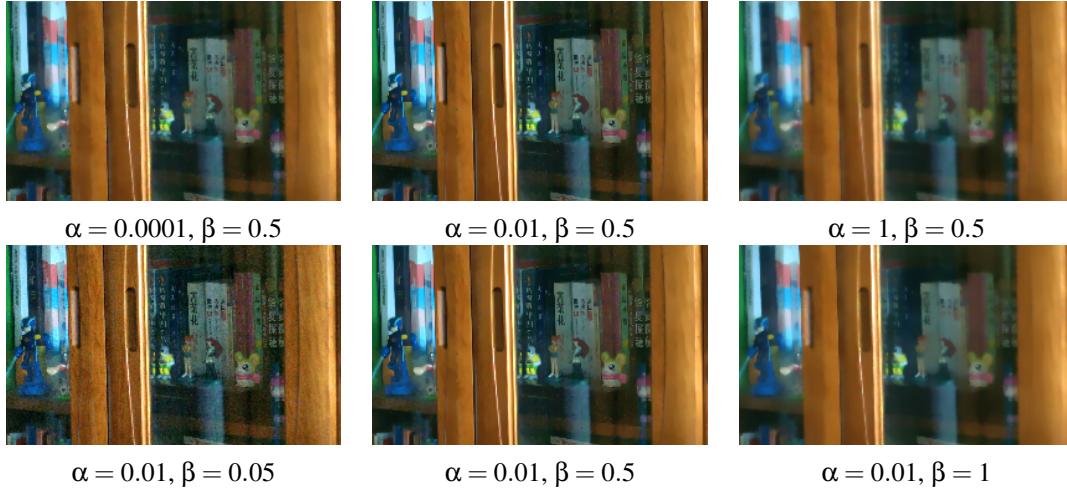
Figure 3: Visual impact of the trade-off parameters α and β in (3) on the final enhanced image. Larger values of α or β result in an over-smoothed image, as can be appreciated in the third column. On the other hand, when the role of the regularization term is less relevant, as it is the case for β = 0.05, the noise is enhanced in the final result.

$\mathcal{N}(x)$ denote a neighbourhood around $x \in \Omega$. Then, $\omega(x, y)$ is defined as in (5) if $y \in \mathcal{N}(x)$, and zero otherwise. The normalization factor is finally given by

$$\Gamma(x) = \int_{\mathcal{N}(x)} \exp\left(-\frac{|x-y|^2}{h_{\text{spt}}^2} - \frac{d\left(L(x), L(y)\right)}{h_{\text{sim}}^2}\right) dy.$$

3.3 Enhanced Image

Once we obtain the illumination and the reflectance, we need to adjust the lighting by applying a gamma correction with parameter $\gamma > 0$ to T, helping us address the over-saturation problem. This transformation involves the following operation at each pixel:

$$T'(x) = S\left(\frac{T(x)}{S}\right)^{\gamma}, \qquad (6)$$

where S is a constant typically set to 1 to ensure that the inputs and outputs are within the same range. Finally, the enhanced image is computed as $L' = R \circ T'$.

4 PRIMAL-DUAL OPTIMIZATION

In the discrete setting, $L, R \in \mathbb{R}^{N \times C}$ and $T \in \mathbb{R}^N$, where N is the number of pixels and C is the number of channels. Both $\nabla T \in \mathbb{R}^{N \times 2}$ and $\nabla R \in \mathbb{R}^{N \times C \times 2}$ are computed via forward differences and Neumann boundary conditions, and denoted for each pixel i and channel k by $(\nabla T)_i = ((\nabla T)_{i,1}, (\nabla T)_{i,2})$ and $(\nabla R)_{i,k} = ((\nabla R)_{i,k,1}, (\nabla R)_{i,k,2})$, respectively.

Let M be the size of the neighborhood around each pixel where the weights of the NLVTV regu-

larization term are nonzero. The nonlocal gradient $\nabla_{\omega} R \in \mathbb{R}^{N \times C \times M}$, denoted for each pixel i and channel k by $(\nabla_{\omega} R)_{i,k} = ((\nabla_{\omega} R)_{i,k,1}, \ldots, (\nabla_{\omega} R)_{i,k,M})$, is defined as $(\nabla_{\omega} R)_{i,k,j} = \sqrt{\omega_{i,j}}\left(R_{j,k} - R_{i,k}\right)$, where $\{\omega_{i,j}\}$ contains the discretization of the weights (5). In practice, the weight of the reference pixel is set to the maximum of the weights in the neihbourhood, i.e., $\omega_{i,i} = \max_{1 \leq j \leq M} \omega_{i,j}$. This setting avoids the excessive weighting of the reference pixel.

Both minimization problems (2) and (3) are convex but non-smooth. To find a global optimal solution, we use the first-order primal-dual algorithm introduced in (Chambolle and Pock, 2011). To do so, we rewrite each problem in a saddle-point formulation by introducing dual variables. The algorithm consists of alternating a gradient ascent in the dual variable, a gradient descent in the primal variable and an over-relaxation for convergence purposes. The gradient steps are given in terms of the proximity operator, which is defined for any proper convex function φ as $\text{prox}_{\tau}\varphi(x) = \arg\min_y\{\varphi(y) + \frac{1}{2\tau}\|x - y\|_2^2\}$. The efficiency of the algorithm is based on the assumption that proximity operators have closed-form representations or can be efficiently solved. For all details on convex analysis omitted in this section, we refer to (Chambolle and Pock, 2016).

4.1 Estimation of the Illumination

The discrete variational model related to (2) is

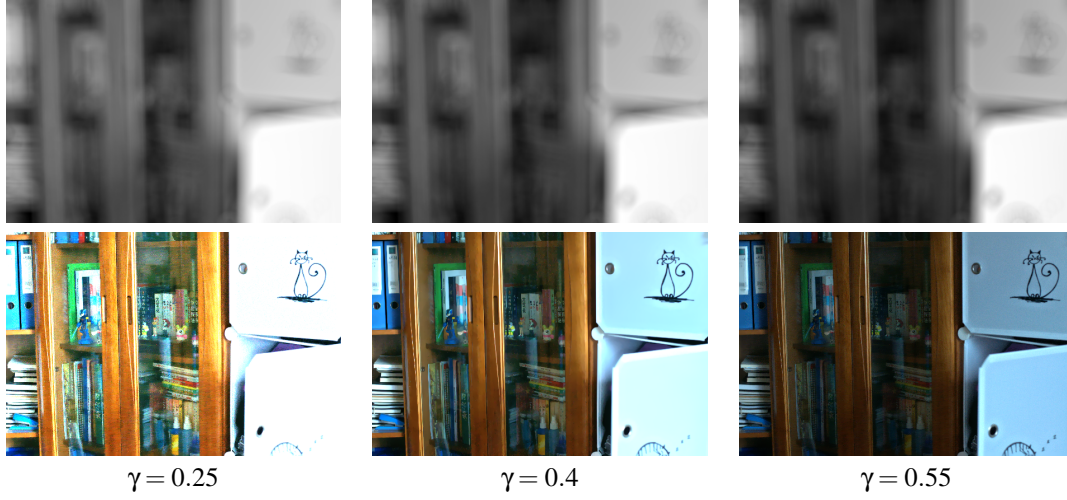$$\min_{T \in \mathbb{R}^N} \|\nabla T\|_1 + \lambda \|T - \hat{T}\|_2^2, \qquad (7)$$

| $\gamma = 0.25$ | $\gamma = 0.4$ | $\gamma = 0.55$ |

Figure 4: Study of the effect of the gamma correction (6) with parameter γ. In the first row, we display the γ-corrected illuminations and the second row contains the resulting enhanced images. We observe that an excessive gamma correction ($\gamma = 0.25$) leads to a saturated image, while a less significant transformation ($\gamma = 0.55$) results in an overly dark image.

where $\|\nabla T\|_1 = \sum_{i=1}^N |(\nabla T)_i|$. The saddle-point formulation of (7) is given by

$$\min_{T \in \mathbb{R}^N} \max_{p \in \mathcal{P}} \langle \nabla T, p \rangle - \delta_{\mathcal{P}}(p) + \lambda \|T - \tilde{T}\|_2^2,$$

where $\mathcal{P} = \{p \in \mathbb{R}^{N \times 2} : |p_{i,:}| \le 1, \forall i\}$ and $\delta_{\mathcal{P}}$ is the indicator function of $\mathcal{P}$.

Therefore, T is computed through the following primal-dual iterates:

$$\begin{cases} p_{i,j}^{n+1} = \dfrac{p_{i,j}^n + \sigma(\nabla \overline{T}^n)_{i,j}}{\max\left(1, |p_i^n + \sigma(\nabla \overline{T}^n)_i|\right)}, \\[2mm] T^{n+1} = \dfrac{T^n + \tau \operatorname{div} p^{n+1} + \tau \lambda \hat{T}}{1 + \tau \lambda}, \\[2mm] \overline{T}^{n+1} = 2T^{n+1} - T^n. \end{cases}$$

4.2 Estimation of the Reflectance

The discretization of the variational model (3) is

$$\beta \|\nabla_\omega R\|_1 + \frac{\alpha}{2}\|\nabla R - G\|_2^2 + \frac{1}{2}\|R - R_0\|_2^2, \quad (8)$$

where $\|\nabla_\omega R\|_1 = \sum_{i=1}^N \sqrt{\sum_{k=1}^C |(\nabla_\omega R)_{i,k}|^2}$ and $\|\cdot\|_2$ applies across channel and pixel dimensions.

The NLVTV term is treated analogously to the TV case. We also need to dualize the α-term since its proximity operator has no closed-form. By taking into account that $\frac{\alpha}{2}\|x\|_2^2 = \sup_y \langle x, y \rangle - \frac{1}{2\alpha}\|y\|_2^2$, the saddle-point formulation of (8) is

$$\min_{R \in \mathbb{R}^{N \times C}} \max_{p \in \mathbb{R}^{N \times C \times 2}, q \in Q} \langle \nabla R, p \rangle + \langle \nabla_\omega R, q \rangle$$
$$- \frac{1}{2\alpha}\|p - G\|_2^2 - \delta_Q(q) + \frac{1}{2}\|R - R_0\|_2^2,$$

with $Q = \{q \in \mathbb{R}^{N \times C \times M} : \sum_{k=1}^C \sum_{j=1}^M q_{i,k,j}^2 \le \beta^2, \forall i\}$.

Therefore, R is computed through the following primal-dual iterates:

$$\begin{cases} p^{n+1} = \dfrac{\alpha\left(p^n + \sigma \nabla \overline{R}^n\right) + \sigma G}{\alpha + \sigma}, \\[2mm] q_{i,k,j}^{n+1} = \dfrac{\beta\left(q_{i,k,j}^n + \sigma(\nabla_\omega \overline{R}^n)_{i,k,j}\right)}{\max\left(\beta, |q_i^n + \sigma(\nabla_\omega \overline{R}^n)_i|\right)}, \\[2mm] R^{n+1} = \dfrac{R^n + \tau \operatorname{div} p + \tau \operatorname{div}_\omega q + \tau R_0}{1 + \tau}, \\[2mm] \overline{R}_i^{n+1} = 2R_i^{n+1} - R_i^n. \end{cases}$$

5 ANALYSIS AND EXPERIMENTS

In this section, we analyze the performance of the proposed method for low-light image enhancement. Figure 1 displays the pairs of low-light and ground-truth images from the LOL dataset (Wei et al., 2018) used in the experiments. We have also used *Lamp* from (Guo et al., 2017), a natural low-light image.

5.1 Ablation Study

Figure 2 illustrates the impact of the trade-off parameter λ in the variational model (2). We observe that a piecewise smooth illumination is obtained in all cases. The slight variation in the illumination is amplified in the reflectance maps and the enhanced images, resulting in darker or brighter images, depending on whether more or less weight is given to the fidelity term compared to the regularization term.
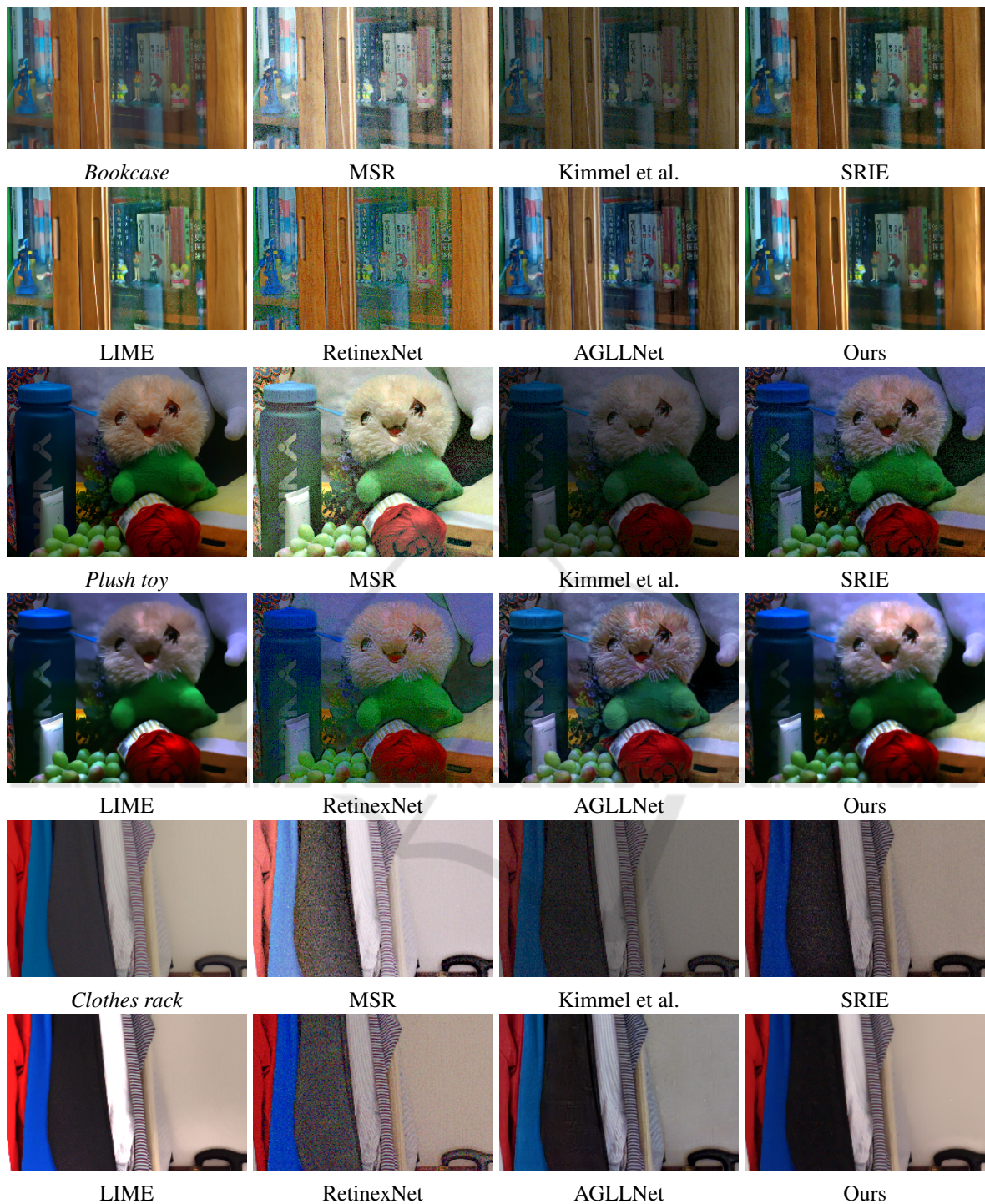
Figure 5: Comparison between state-of-the-art techniques and our method on dataset in Figure 1. We observe that MSR, SRIE and RetinexNet are not robust to noise and exhibit color issues in all experiments. The method by Kimmel et al. is not able to correctly remove the effect of the illumination, while LIME produces oversaturated results. AGLLNet produces greyish images and introduces color artifacts as seen for instance in the blue bottle and the red ball of yarn. Our method provides the best compromise between discounting the illumination effect, avoiding the amplification of noise, and preserving the color and geometry structure of the scene.
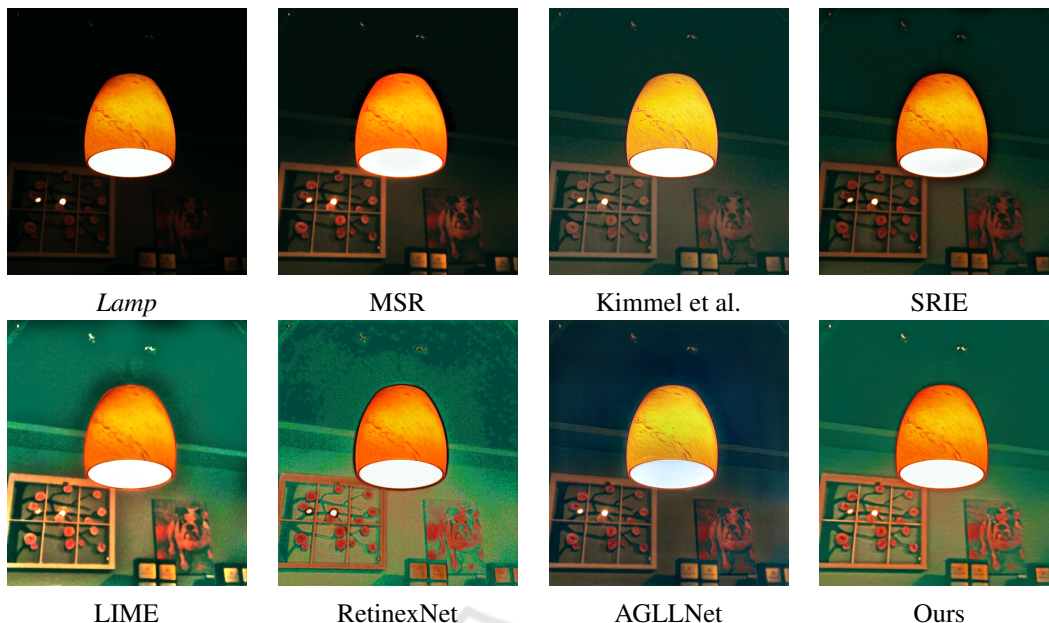
Figure 6: Comparison between state-of-the-art methods and our proposal on a natural low-light image. We observe that only LIME, RetinexNet and our method are able to remove the effect of the illumination. However, LIME and RetinexNet are affected by noise and also produce enhanced images with artifacts, like the halo surrounding the lamp.

In Figure 3, we discuss about the influence of the trade-off parameters α and β in (3) on the enhanced image produced by the proposed method. We observe that larger values of α or β result in an over-smoothed image. On the other hand, when the role of the regularization term is less relevant, as it is the case for $\beta = 0.05$, the noise is amplified.

Gamma correction is an essential tool for adjusting the lighting, as shown in Figure 4. Indeed, we observe how varying γ significantly affects the final image: an excessive gamma correction ($\gamma = 0.25$) leads to a saturated image, while a less significant transformation ($\gamma = 0.55$) results in an overly dark image.

5.2 Comparison with the State of the Art

We compare our method with Multiscale Retinex (MSR) (Jobson et al., 1997), Kimmel et al. (Kimmel et al., 2001), SRIE (Fu et al., 2016b), LIME (Guo et al., 2017) and the deep learning techniques RetinexNet (Wei et al., 2018) and AGLLNet (Lv et al., 2021). Kimmel et al. and LIME have been implemented by ourselves, while SRIE is sourced from (Ying et al., 2017) and MSR from (Petro et al., 2014). The trained networks of RetinexNet and AGLLNet are provided by the authors on their webpages. The most suitable parameters for state-of-the-art and our method have been chosen based on visual evaluation.

Table 1: Quantitative evaluation on results in Figure 5.

	PSNR $\uparrow$	SSIM $\uparrow$
MSR	12.41	0.7229
Kimmel et al.	14.27	0.8287
SRIE	17.27	0.8483
LIME	18.09	0.8592
RetinexNet	17.56	0.7819
AGLLNet	16.82	0.8661
Ours	**20.08**	**0.8868**

Figure 5 displays a comparison among all methods on *Bookcase*, *Clothes rack* and *Plush toy*. We observe that MSR, SRIE and RetinexNet are not robust to noise and exhibit color issues in all cases. The method by Kimmel et al. is not able to correctly remove the effect of the illumination, while LIME tends to oversaturate the scene. AGLLNet produces greyish images, introduces color artifacts, as seen in the blue bottle and the red ball of yarn in *Plush toy*, and modifies the texture of the reference image, as seen in the wood of *Bookcase*. Our method provides the best compromise between discounting the illumination effect, avoiding the amplification of noise, and preserving the color and geometry structure of the scene.

We also evaluate the performance of all methods in terms of PSNR and SSIM. Table 1 displays the average values on the results in Figure 5. Our method outperforms the others in terms of both metrics.

An additional analysis has been performed with the natural low-light image *Lamp* in Figure 6. Only

LIME, RetinexNet and our method are able to remove the effect of the illumination. However, LIME and RetinexNet are affected by noise and also produce artifacts, like the halo surrounding the lamp.

6 CONCLUSION

In this paper, we have proposed a low-light image enhancement method that estimates illumination and reflectance separately using variational models. In particular, we have introduced a contrast-invariant nonlocal regularization term for recovering fine details in the reflectance component. The experiments have shown that our method obtains state-of-the-art results and performs well in terms of noise reduction, color recovery, geometry and texture preservation.

ACKNOWLEDGEMENTS

REFERENCES

Buades, A., Lisani, J.-L., Petro, A. B., and Sbert, C. (2020). Backlit images enhancement using global tone mappings and image fusion. *IET Image Processing*, 14(2):211–219.

Chambolle, A. and Pock, T. (2011). A first-order primal-dual algorithm for convex problems with applications to imaging. *Journal of Mathematical Imaging and Vision*, 40:120–145.

Chambolle, A. and Pock, T. (2016). An introduction to continuous optimization for imaging. *Acta Numerica*, 25:161–319.

Duran, J., Buades, A., Coll, B., and Sbert, C. (2014). A nonlocal variational model for pansharpening image fusion. *SIAM Journal on Imaging Sciences*, 7(2):761–796.

Fu, X., Zeng, D., Huang, Y., Liao, Y., Ding, X., and Paisley, J. (2016a). A fusion-based enhancing method for weakly illuminated images. *Signal Processing*, 129:82–96.

Fu, X., Zeng, D., Huang, Y., Zhang, X., and Ding, X. (2016b). A weighted variational model for simultaneous reflectance and illumination estimation. *CVPR*, pages 2782–2790.

Gilboa, G. and Osher, S. (2009). Nonlocal operators with applications to image processing. *Multiscale Modeling & Simulation*, 7(3):1005–1028.

Gu, Z., Li, F., and Lv, X.-G. (2019). A detail preserving variational model for image retinex. *Applied Mathematical Modelling*, 68:643–661.

Guo, X., Yu, L., and Ling, H. (2017). Lime: Low-light image enhancement via illumination map estimation. *IEEE Transactions on Image Processing*, 26(2):982–993.

Jobson, D., Rahman, Z., and Woodell, G. (1996). Properties and performance of a center/surround retinex. *TIP*, 6(3):451–462.

Jobson, D., Rahman, Z., and Woodell, G. (1997). A multiscale retinex for bridging the gap between color images and the human observation of scenes. *IEEE Transactions on Image Processing*, 6(7):965–976.

Kimmel, R., Elad, M., Shaked, D., Keshet, R., and Sobel, I. (2001). A variational framework for retinex. *Int. J. Comput. Vis.*, 52(1):7–23.

Land, E. H. and McCann, J. J. (1971). Lightness and retinex theory. *Journal of the Optical Society of America*, 61(1):1–11.

Li, M., Liu, J., Yang, W., Sun, X., and Guo, Z. (2018). Structure-revealing low-light image enhancement via robust retinex model. *IEEE Transactions on Image Processing*, pages 2828–2841.

Lv, F., Yu, L., and Lu, F. (2021). Attention guided low-light image enhancement with a large scale low-light simulation dataset. *International Journal of Computer Vision*, pages 2175—-2193.

Ma, W. and Osher, S. (2012). A tv bregman iterative model of retinex theory. *Inverse Problems and Imaging*, 6(4):697–708.

Morel, J. M., Petro, A. B., and Sbert, C. (2010). A pde formalization of retinex theory. *IEEE Transactions on Image Processing*, 19(11):2825–2837.

Ng, M. K. and Wang, W. (2011). A total variation model for retinex. *SIAM J. Imag. Sci.*, 4(1):345–365.

Paul, A., Bhattacharya, P., and Maity, S. P. (2022). Histogram modification in adaptive bi-histogram equalization for contrast enhancement on digital images. *Optik*, 259:168899.

Petro, A. B., Sbert, C., and Morel, J. M. (2014). Multiscale retinex. *Image Processing On Line*, pages 71–88.

Rudin, L. I., Osher, S., and Fatemi, E. (1992). Nonlinear total variation based noise removal algorithms. *Physica D: Nonlinear Phenomena*, 60(1):259–268.

Thepade, S. D., Ople, M., Mahindra, V., Kulye, V., and Jamdar, S. (2021). Low light image contrast enhancement using blending of histogram equalization based methods bbhe and bpheme. In *2021 International Conference on Disruptive Technologies for Multi-Disciplinary Research and Applications (CENTCON)*, volume 1, pages 259–264.

Wang, W., Wu, X., and snd Z. Guo, X. Y. (2020). An experiment-based review of low-light image enhancement methods. *IEEE Access*, 8:87884–87917.

Wei, C., Wang, W., Yang, W., and Liu, J. (2018). Deep retinex decomposition for low-light enhancement. *BMVC*.

Ying, Z., Li, G., and Gao, W. (2017). A bio-inspired multi-exposure fusion framework for low-light image enhancement.